https://doi.org/10.5194/egusphere-2026-3420
Preprint. Discussion started: 6 July 2026

Stability constraining the radiation-driven convective anvil outflow

Zhenquan Wang [1]

[1]School of Atmospheric Physics, Nanjing University of Information Science and Technology, Nanjing, China

Corresponding author: Zhenquan Wang (zhqwang@nuist.edu.cn)

Abstract. Anvil clouds outflowing from the convection top interact strongly with radiation. The anvil formation is driven by radiation and simultaneously modulates radiation. Since the convective anvil outflow process has not been well resolved from observations, the hypothesized anvil-radiation feedback processes are lack of adequate evidence to be further refined. In this work, by combining the advantages of geostationary satellites for identifying convection producing anvil clouds and the A-Train polar-orbit satellites for the cross section of the radiation heating the anvil, the real-world convective anvil outflow is resolved to further refine the previously hypothesized process of the radiation driving the anvil outflow. The results show that the destabilization of the longwave radiative cooling at the cloud top only partially explains the anvil outflow dynamics at relatively lower levels, and that the shortwave radiative heating and its destabilization can strongly enhance the outflow at higher levels. Nevertheless, notably, the role of the radiation driving the anvil outflow is strongly constrained by its environmental stability and its vertical gradient. In the vertical, the primary radiation-driven anvil outflow is constrained between the levels of the minimum stability and the maximum stability gradient approximately 12-14 km. Less stable environment or upward-shifting of the minimum stability makes the anvil produced at a higher level. Overall, this work clarifies the process of the anvil outflow driven by radiation but constrained by environmental stability and provides a novel stability constraint on the anvil-radiation feedback.

1 Introduction

Convective cloud systems are normally organized by a narrow pillar of deep convective cores with heavy precipitation and a large spread of outflowing non-precipitating anvil clouds (Houze, 2004; Yuan and Houze, 2010; Yuan et al., 2011; Deng et al., 2016). Normally, although these outflowing anvil clouds only account for a small portion of total convective moisture (Moorthi and Suarez, 1992; Del Genio and Kovari, 2002; Clement and Soden, 2005; Xu et al., 2006), the anvil can extend out to approximately 5 times the equivalent radius of precipitating cores to cover a large area (Riihimaki and Mcfarlane, 2010; Igel et al., 2014) and can evaporate slower than low-level clouds to persist a long lifetime (Seeley et al., 2019; Zheng et al., 2025). This contributes to the top-heavy peak of the vertical cloud distribution for convective systems, which is usually referred to as the anvil. For the outflowing anvil clouds, they can strongly reflect solar shortwave (SW) radiation and also strongly trap surface outgoing longwave (LW) radiation. Consequently, their SW and LW radiative effects nearly cancel each other out and the final net radiation is similar to that of the non-convective regions (Kiehl, 1994). Importantly, this radiative near cancellation can be easily disturbed by changes of the anvil altitude (Kiehl, 1994; Hartmann and Larson, 2002; Zelinka and Hartmann, 2010), area coverage (Lindzen et al., 2001; Mauritsen and Stevens, 2015; Bony et al., 2016), structure (Berry and Mace, 2014; Hartmann and Berry, 2017; Raghuraman et al., 2024; Sokol et al., 2024) and diurnal variation (Yin and Porporato, 2019; Gasparini et al., 2021; Wang, 2025).

To explain the anvil responses to environmental changes, the mass and energy conservations are the fundamental physical constraints. In tropics, according to the thermodynamical energy function with the weak temperature gradient (WTG) approximation (Sobel et al., 2001), diabatic heating is balanced by adiabatic vertical motions at the equilibrium state (Mapes and Houze, 1995; Folkins, 2002; Folkins and Martin, 2005; Thompson et al., 2017):

$$\omega = -\frac{Q}{s}, \quad (1)$$

https://doi.org/10.5194/egusphere-2026-3420
Preprint. Discussion started: 6 July 2026

where ω is the vertical velocity in pressure coordinates, S is the stability (i.e., $-\frac{T}{\theta}\frac{\partial\theta}{\partial p}$ in pressure coordinates or $\frac{T}{\theta}\frac{1}{\rho g}\frac{\partial\theta}{\partial z}$ in height coordinates), and Q is the diabatic heating rate of latent heat release and radiation. Specifically, condensational and radiative heating of convective clouds is balanced by adiabatic cooling through ascent, while radiative cooling of clear skies is balanced by adiabatic heating through subsidence. This configuration induces mesoscale circulations between convective and clear-sky regions, to further lift and spread high-level ice clouds (Gray and Jacobson, 1977; Nicholls, 2015; Wall et al., 2020; Hartmann and Larson, 2002). This provides fundamental understanding on the relationship among convective anvil outflows, thermodynamics and circulations.

By combining Eq. (1) with the continuity function, the convective divergence (D) can be expressed as:

$$D = -\frac{\partial\omega}{\partial p} = \frac{\partial}{\partial p}\left(\frac{Q}{S}\right). \quad (2)$$

For mass conservation, D and clear-sky convergence (C) should be compensated with each other at the equilibrium state (i.e., $C = D$). Compared with the convective cloud processes behind D in Eq. (2) that are still parameterized imperfectly (Rennó et al., 1994; Clement and Soden, 2005; Suzuki et al., 2013; Zhao, 2014; Zhao et al., 2016; Blossey et al., 2007; Matsui et al., 2009; Powell et al., 2012; Bretherton, 2015; Feng et al., 2018; Atlas et al., 2024), the mechanisms behind C are relatively simpler without cloud-radiation interactions and complicated microphysical processes. Thereby, instead of investigating D directly, C is usually used to diagnose D, provided mass conservation at steady state (Hartmann and Larson, 2002; Bony et al., 2016; Saint-Lu et al., 2020; Zelinka and Hartmann, 2010). Specifically, the anvil outflow can be considered to be indirectly constrained by the clear-sky radiative heating and clear-sky stability that contribute to C, e.g., the Fixed Anvil-top Temperature (FAT) hypothesis (Hartmann and Larson, 2002), the Proportionally Higher Anvil Temperature (PHAT) hypothesis (Zelinka and Hartmann, 2010) and the Stability Iris effect (Bony et al., 2016; Saint-Lu et al., 2020). Essentially, these hypotheses provide important thermodynamical factors directly (indirectly) constraining C (D).

Understandings on the thermodynamical processes directly controlling convective outflows are still incomplete and some relevant hypothesized processes for building the model parameterization are still lack of adequate observational evidences. Lilly (1988) hypothesized a two-stage process for the anvil outflow dynamics. Initially, for the intrusion of the outflowing air of nearly neutral stability into the stably stratified environment, the top (base) of the outflow is colder (warmer) than its corresponding environment to sink (rise). As a result, the outflow would be flattened and spread by the environmental stability for collapse from the three-dimensional to quasi-two-dimensional regimes (Schooley, 1967). It has been argued that the second stage of the anvil outflow is primarily driven by the radiative destabilization (Lilly, 1988; Wang, 2025). Particularly, the LW radiative cooling at the cloud top can destabilize the anvil layer to generate the turbulent overturing and promote the outflow. Thus, a radiative-convective mixed layer was thereby hypothesized for explaining the anvil outflow (Lilly, 1988). Simply, this hypothesis can also be understood based on Eq. (2) that the vertical peak of D is determined by the coupling impact of S and Q profiles and their vertical gradients. Although the nighttime anvil outflow might be primarily driven by the LW radiative destabilization, daytime anvil clouds are strongly heated and destabilized by SW radiation but the mechanism for the SW radiation driving the anvil outflow is not clear. Additionally, for either the LW or SW radiation, the coupling impact of S and Q in Eq. (2) implies that the anvil-radiation interaction would be constrained by the environmental stability, but this constraint has been incompletely understood in the previously hypothesized anvil outflow processes.

Overall, the anvil outflow process hypothesized in Lilly (1988) and the Eq. (2) both provide the fundamental physics for understanding the anvil-radiation interaction. But the mechanism for the SW radiation driving the anvil outflow and the stability constraint on the radiation-driven anvil outflow need further investigation. With advances in the satellite remote-sensing technologies, radiative-transfer theories and cloud microphysical studies over recent decades, the necessary quantities of LW and SW heating profiles for clouds can be well measured (Kato et al., 2011). Moreover, grounded on the combination of the geostationary satellites (GEOs) for identifying convective spatial organizations and tracking and the polar-orbiting satellites with active sensors for the cross section of clouds and their radiative structure (Wang and Yuan, 2024; Wang, 2025),

https://doi.org/10.5194/egusphere-2026-3420
Preprint. Discussion started: 6 July 2026

the anvil outflow and its accompanied radiative heating can be well presented from observations. Thus, in this work, on the basis of the radiative-driven anvil outflow layer (RAOL) hypothesized in Lilly (1988), a refined stability constrained RAOL for how the anvil outflow is driven by the LW and SW radiation and constrained by environmental stability is further clarified and examined based on satellite observations.

2 Data and Methods

2.1 GEO-A-Train merged (GATM) convective cloud data product

The GATM convective cloud data product was developed in Wang and Yuan (2024) and Wang (2025). The purpose of the GATM is to resolve the convective anvil outflow and its accompanying radiative structures from the combination of advantages from multi-satellite observations. To be specific, based on the advantages of the GEOs for tracking, the tropical complex convective organizations (CCOs) are identified from the 1-hour infrared brightness temperature (BT) images of the 0.05° resolution. And in CCOs, single-cold-core organization segments (OSs) are tracked separately (Wang and Yuan, 2024). The OSs with heavy precipitation exceeding 6 mm h^{-1} of over 1000 km^2, the peaking convective core colder than 220 K and a duration over 5 hours are considered mesoscale convective systems (MCSs). These MCSs represent the isolated deep convective activities in the CCOs and explain most of the CCO precipitation and anvil clouds (Wang and Yuan, 2024).

Secondly, based on the advantages of the A-Train Constellation for providing the cross section of the convective anvil outflow, cloud and radiance structures can be measured by a combination of multiple instruments (Stephens et al., 2002; L'ecuyer and Jiang, 2010), including Cloud-Aerosol Lidar and Infrared Pathfinder Satellite Observations (CALIPSO) Cloud-Aerosol Lidar with Orthogonal Polarization (CALIOP), CloudSat Cloud Profiling Radar (CPR), Clouds and the Earth's Radiant Energy System (CERES) and the Moderate Resolution Imaging Spectroradiometer (MODIS). In the CALIPSO-CloudSat-CERES-MODIS (CCCM) product developed in Kato et al. (2011), the capabilities of these instruments are merged for comprehensive cloud-radiation-interaction observations. The cloud fraction at each height is computed as the percentage of clouds detected by CALIOP and CPR over the CERES footprint of the resolution of 20 km (Kato et al., 2010; Kato et al., 2011). In the vertical direction, the peak level of cloud fraction is regarded as the main level of cloud outflow to form the anvil (Z_{anvil}). The vertical resolution of cloud fraction and irradiance profiles is 240 m. Atmospheric temperature and pressure profiles provided in the CCCM are from the Goddard Earth Observing System (GEOS-5) Data Assimilation System reanalysis.

With the combination of the GEO for the MCS identification and tracking and the CCCM for the MCS cloud and radiative cross sections, the structures for the anvil outflow and its accompanying radiative destabilization can be presented based on the GATM. Here, non-precipitating anvil clouds in the GATM are identified by the GEO infrared image pixel of BT colder than 260 K and precipitation rate less than 1 mm h^{-1} (Yuan and Houze, 2010). The tropical western Pacific (TWP, 130°W-170°E, 15°S-15°N) is selected as the study region and only oceanic MCSs are considered. MCSs and anvil clouds are common in this region but the net radiation shows small differences compared with nonconvecting regions (Hartmann, 2016; Hartmann and Berry, 2017; Wall et al., 2018; Wall et al., 2020). Thus, it is a typical region for investigating the oceanic deep convection and its anvil outflow. Notably, owing to the sun-synchronous orbit of the A-Train Constellation, only the cross sections of MCSs around 1:30 and 13:30 local time are available. To filter out the impact from the seasonal cycle, the observational time is limited in June, July and August between 2006 and 2011.

2.2 Reanalysis

The European Centre for Medium-Range Weather Forecasts (ECMWF) provides the fifth-generation atmospheric reanalysis (ERA5) of 1-hour temporal resolution and 0.5° spatial resolution. Temperature and geopotential profiles are retrieved from the ERA5. θ is computed via temperature and pressure and then the dθ/dz profiles are computed at the ERA5

https://doi.org/10.5194/egusphere-2026-3420
Preprint. Discussion started: 6 July 2026

half level. As suggested in Wang and Yuan (2025), the estimated anvil-outflow stability (EAS) is defined as the minimum dθ/dz in the upper troposphere (between 5-18 km):

$$EAS = (\frac{d\theta}{dz})_{min}. \quad (3)$$

It has been demonstrated that the EAS represents the control of the upper-tropospheric stability on convective anvil outflow and thereby a strong high-cloud controlling factor. Owing to the coarse vertical resolution of the ERA5 profile, the EAS cannot be derived as accurate as the radiosonde measures. Nevertheless, a strong negative correlation between daily high-cloud area coverage and the ERA5-based EAS exceeds −0.6 over the Tropical Western Pacific (TWP). EAS and its height (Z_{EAS}) are derived from the ERA5 atmospheric profiles and have 1-hour temporal resolution and 0.5° spatial resolution. These metrics are allocated to the closest A-Train footprint in CCCM within 0.25° and half an hour.

3 How the stability constrains the radiation-driven anvil outflow

To explain the radiation-driven anvil outflow and the constraint of stability on it, Eq. (2) can be further expressed as:

$$D = \frac{1}{S}\frac{\partial R}{\partial p} + R\frac{\partial}{\partial p}\left(\frac{1}{S}\right). \quad (4)$$

Here, R represents the radiative heating. Notably, for the high-level non-precipitating anvil clouds, the diabatic heating is mainly contributed by the radiation (Lilly, 1988; Gasparini et al., 2019). Positive and negative $\frac{\partial R}{\partial p}$ values represent the radiative destabilization and stabilization, respectively. Based on this formulation, the divergent outflow is contributed by the collective impacts of R, $\frac{1}{S}$ and their vertical gradients. Given the hypothesized anvil outflowing processes by Lilly (1988), Eq. (4) further manifests that the impacts of $\frac{\partial R}{\partial p}$ and R on the RAOL are constrained by $\frac{1}{S}$ and its gradient, respectively. Thus, two terms for the stability constrained RAOL (SCRAOL) of radiative destabilization ($\frac{1}{S}\frac{\partial R}{\partial p}$) and heating ($R\frac{\partial}{\partial p}\left(\frac{1}{S}\right)$) can be recognized and defined as the $SCRAOL_{RD}$ and $SCRAOL_{RH}$, respectively. $SCRAOL_{RD}$ and $SCRAOL_{RH}$ represent the RAOLs driven by radiative destabilization and heating but constrained by environmental stability, respectively.

In the vertical direction, the LW cooling normally occurs at the cloud top and the SW radiation heats the upper portion of clouds with a strong diurnal cycle. Thus, R and $\frac{\partial R}{\partial p}$ are closely associated with the convective cloud vertical development and the diurnal cycle of insolation. For the environmental stability, the peak level of $\frac{1}{S}$ is less variable and normally occurs at ~12 km (Gettelman and Forster, 2002; Wang and Yuan, 2025). This strong vertical variation of stability implies variable constraints on the anvil production at different height, which may shape the top-heavy high-level cloud systems. In this way, Eq. (4) seems to be determined by the coupling of the convective cloud development, diurnal cycle of insolation and environmental stability.

To resolve the coupling impact of the convection, radiation and environmental stability for the anvil outflow, their profiles based on the GATM are presented in Figure 1 and 2. Here, owing to the limitation of the sun-synchronous orbit of the A-Train Constellation, only the profiles of June, July and August at 13:30 local time over the TWP are focused on. This implies that the insolation is nearly fixed to basically exclude the impacts from the diurnal and seasonal cycles. In this case, the radiative heating profiles are primarily related to the vertical development of convective clouds and its anvil-outflow structure.

The SCRAOLs determined by the cloudy (Figure 1a-d and Figure 2a-c) and clear skies (Figure 1e-h and Figure 2d-f) are discussed, respectively. For the cloudy sky, the SCRAOL is directly driven by the coupling of convection, radiation and environmental stability, which corresponds to the anvil outflowing processes hypothesized in Lilly (1988). On the other hand, the SCRAOL can be indirectly constrained by the clear-sky convergence for circulations and mass conservation, which corresponds to the hypotheses of the FAT, PHAT and stability iris effects (Hartmann and Larson, 2002; Zelinka and Hartmann,

https://doi.org/10.5194/egusphere-2026-3420
Preprint. Discussion started: 6 July 2026

2010; Bony et al., 2016).

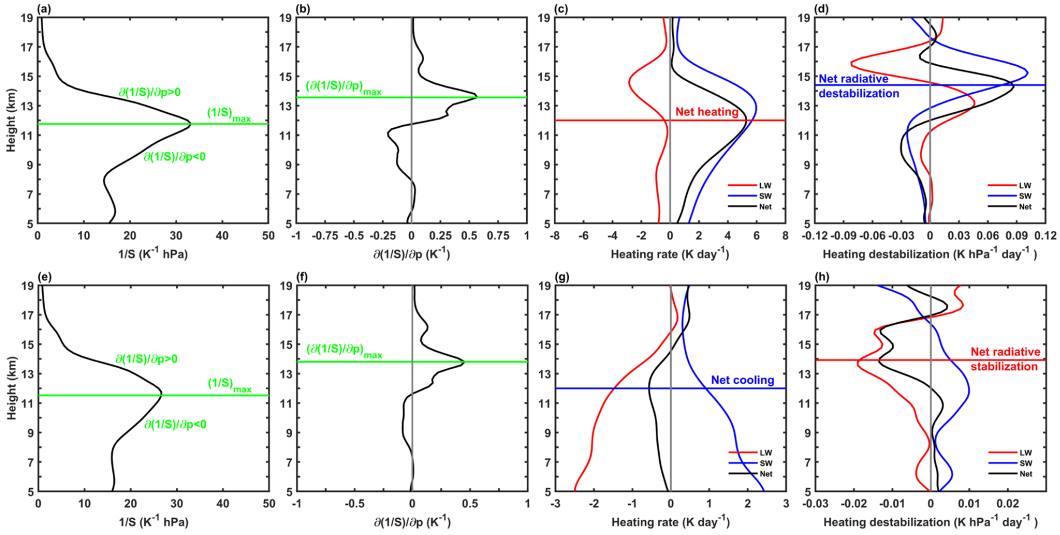

160

Figure 1. Stability, radiative heating and their vertical gradient profiles at 13:30 local time based on the GATM. (a)-(d) The composites of $\frac{1}{S}$, $\frac{\partial}{\partial p}\left(\frac{1}{S}\right)$, Q and $\frac{\partial Q}{\partial p}$ profiles for non-precipitating anvil clouds, respectively. (e-h) Similar to (a-d) but for the clear sky. The peaking levels and their physical meanings are marked in figures. In (c) and (g), red, blue and black lines represent the LW, SW and Net radiative heating, respectively. In (d) and (h), red, blue and black lines represent the LW, SW and Net radiative destabilization, respectively.

165

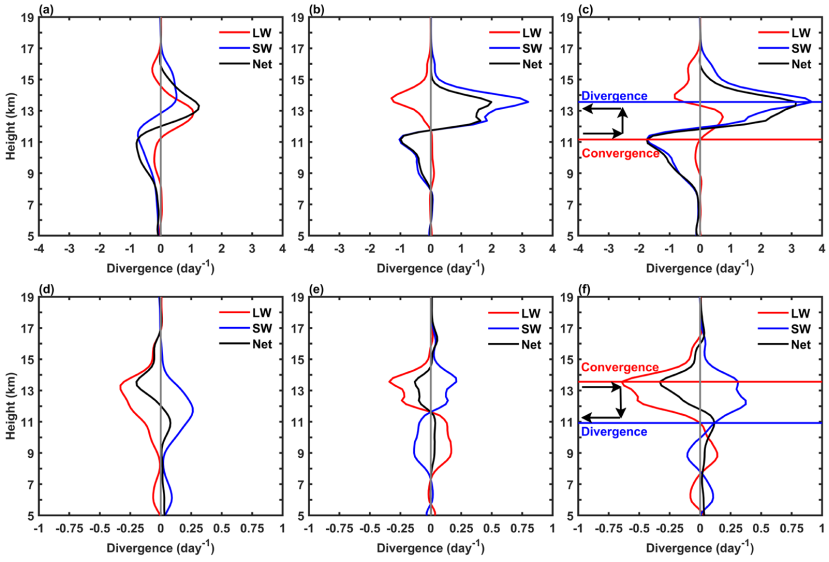

Figure 2. The RAOL at the equilibrium state contributed by the collective impacts of stability, radiative heating and their vertical gradient profiles at 13:30 local time based on the GATM. (a)-(c) The RAOL contributed by the destabilization term $\left(\frac{1}{S}\frac{\partial Q}{\partial p}\right)$, heating term $\left(Q\frac{\partial}{\partial p}\left(\frac{1}{S}\right)\right)$, and both of them for the non-precipitating anvil clouds, respectively. (d)-(f) similar to (a)-(c) but for the clear sky. Red, blue and black lines represent the contribution from LW, SW and Net radiation, respectively.

170

https://doi.org/10.5194/egusphere-2026-3420
Preprint. Discussion started: 6 July 2026

For the non-precipitating anvil clouds, the composites of stability, radiative heating and their vertical gradient profiles are presented in Figures 1a-d. Figure 1a shows that the $\frac{1}{S}$ profile has a maximum point (or the minimum point of S), which is the key characteristic of upper-tropospheric thermal stratification (Folkins, 2002; Gettelman and Forster, 2002; Biondi et al., 2012; Sunilkumar et al., 2013; Xian and Fu, 2015; Sunilkumar et al., 2017; Babu, 2024; Wang and Yuan, 2025). Below the level of the maximum $\frac{1}{S}$, S is more controlled by the convective latent heat release to decease with height and thus $\frac{\partial}{\partial p}\left(\frac{1}{S}\right) < 0$ (Figure 1b). On the other hand, at a higher level, S is more controlled by the radiation to increase vertically and thus $\frac{\partial}{\partial p}\left(\frac{1}{S}\right) > 0$ (Figure 1b). Overall, $\frac{1}{S}$ and $\frac{\partial}{\partial p}\left(\frac{1}{S}\right)$ both have a strong peak in the vertical as shown in Figure 1a and 1b. Based on Eq. (4), stronger their peaks are, stronger constraints on D they have. Wang and Yuan (2025) found that the minimum of stability in the upper troposphere is well correlated with the tropical high-level ice cloud amount. The underlying mechanism for this strong correlation may be explained by the constraint of stability on D.

In Figure 1c, owing to the overwhelmingly stronger SW heating to clouds than LW cooling, the cloudy upper troposphere is ultimately heated. In Figures 1c and 1d, in the upper troposphere, the rapid decrease of the SW heating contributes to the peak of the radiative destabilization. In Eq. (4), the contributions of the radiative destabilization ($\frac{\partial R}{\partial p}$) and heating ($R$) to the anvil outflow are limited by $\frac{1}{S}$ and $\frac{\partial}{\partial p}\left(\frac{1}{S}\right)$, respectively. For the $SCRAOL_{RD}$ ($\frac{1}{S}\frac{\partial R}{\partial p}$, Figure 2a), its peak is contributed by both the LW and SW radiative destabilization. Notably, the SW radiative destabilization is much stronger than the LW destabilization (Figure 1d), but its contribution to the divergent outflow is relatively weaker than that of the LW destabilization (Figure 2a). An explanation is that, in comparison to the LW destabilization, the strong SW radiative destabilization occurs at a higher level (Figure 1d) and is limited by stronger stability (smaller $\frac{1}{S}$ values shown Figure 1a). Thus, owing to this strong stability constraint, the SW radiative destabilization contributes to weaker divergent outflow compared with the LW destabilization. This implies that the role of the radiative destabilization is strongly constrained by the stability. In the vertical, the maximum of $\frac{1}{S}$ is the most favorable height for the radiative-destabilization driven anvil outflow. Away from this level, the impact of the radiative destabilization on the anvil outflow is limited.

For the $SCRAOL_{RH}$ in Figure 2b, it seems that the radiative heating can directly contribute to a strong outflow layer. Notably, this outflow layer driven by the radiative heating (Figure 2b) is stronger than that driven by the radiative destabilization (Figure 2a). According to Eq. (4), the anvil outflow driven by the radiative heating and cooling is constrained by the vertical gradient of $\frac{1}{S}$ (i.e., $\frac{\partial}{\partial p}\left(\frac{1}{S}\right)$). For the regime above the maximum of $\frac{1}{S}$, $\frac{\partial}{\partial p}\left(\frac{1}{S}\right)$ is positive and thus the radiative heating promotes anvil outflow. By further coupling with the rapid increase of S (that corresponds to larger $\frac{\partial}{\partial p}\left(\frac{1}{S}\right)$) in the tropopause layer, the radiative heating drives the strongest $SCRAOL_{RH}$ above the maximum of $\frac{1}{S}$. On the other hand, below the maximum of $\frac{1}{S}$, $\frac{\partial}{\partial p}\left(\frac{1}{S}\right)$ is negative and thus radiative heating (cooling) contributes to the convergence (divergence). This implies that, only when the convective cloud top overshoots the level of the maximum of $\frac{1}{S}$, the radiative heating is responsible for the outflow of anvil clouds. Consequently, between the levels of the maximum of $\frac{1}{S}$ and $\frac{\partial}{\partial p}\left(\frac{1}{S}\right)$, it seems to be the most favorable environment for the radiative-heating driven anvil outflow. Away from this layer, the role of the radiative heating for the anvil outflow is also limited.

Overall, the final anvil outflow in Figure 2c is contributed by the sum of $SCRAOL_{RD}$ and $SCRAOL_{RH}$ of comparable strengths (Figure 2a and 2b) that peak at similar altitudes. Compared with the LW radiation, the SW radiation can contribute to much stronger anvil outflow at higher levels through heating and destabilizing. This might explain the observed diurnal cycle of the convective anvil outflow that has the maximum at the daytime (Wall et al., 2020; Wang, 2025). Additionally, the

https://doi.org/10.5194/egusphere-2026-3420
Preprint. Discussion started: 6 July 2026

stability plays an important role for constraining not only the strength but also the structure of the anvil outflow. As discussed above, owing to the strong constraint of environmental stability on the impacts of radiative heating and destabilization, the final SCRAOL is largely limited between the levels of the maximum of $\frac{1}{S}$ and $\frac{\partial}{\partial p}\left(\frac{1}{S}\right)$.

For the clear sky, it can constrain the anvil outflow through the mass conservation (i.e., $C = D$) (Hartmann and Larson, 2002; Folkins, 2002; Zelinka and Hartmann, 2010; Bony et al., 2016; Saint-Lu et al., 2020). As shown in Figure 2c and 2f, the maximum of convective anvil outflow (Figure 2c) and clear-sky convergence both occur at the altitude of 13.7 km. It seems to form a circulation between the anvil and the clear sky in the upper troposphere, which is consistent with the hypothesized circulation due to the mass conservation (Gray and Jacobson, 1977; Nicholls, 2015; Wall et al., 2020; Hartmann and Larson, 2002). Thus, at the equilibrium state, the height and strength of the clear-sky C can be used to diagnose the convective anvil outflow. Similar to D, the clear-sky C is also explained by the collective impacts of R, $\frac{1}{S}$ and their vertical gradients. Their profiles and coupling impacts on the clear-sky C are presented in Figure 1e-h and Figure 2d-f, respectively.

The FAT hypothesis states that the level of the maximum of the clear-sky convergence (C_{max}, and hereafter the subscript "max" represents the maximum point of a variable in the vertical direction) is explained by the rapid decline of radiative cooling (i.e., radiative stabilization) (Hartmann and Larson, 2002). Consistently, the rapid decline of the clear-sky radiative cooling occurs at 14.0 km (Figure 1g-h) and C_{max} is at 13.7 km (Figure 2f), whose average heights are nearly the same at the mean state with a low bias of only 0.3 km. Nevertheless, the FAT hypothesis is imperfect since merely the impact of $\frac{\partial R}{\partial p}$ in Eq. (4) is focused on (Chae and Sherwood, 2010). The PHAT and the stability iris effect contribute to a refined hypothesis to further take the stability constraint into account, which corresponds to the term $\frac{1}{S}\frac{\partial R}{\partial p}$ in Eq. (4). But, notably, the impact of $R\frac{\partial}{\partial p}\left(\frac{1}{S}\right)$ in Eq. (4) is missing in these hypotheses. Figure 2d and 2e show that the peaks of $\frac{1}{S}\frac{\partial R}{\partial p}$ and $R\frac{\partial}{\partial p}\left(\frac{1}{S}\right)$ of comparable strengths occur at a similar height. This makes the height of C_{max} (Figure 2f) coincidently resemble the height of the maximum $\frac{1}{S}\frac{\partial R}{\partial p}$, but in physics C_{max} should be explained by both the $\frac{1}{S}\frac{\partial R}{\partial p}$ and $R\frac{\partial}{\partial p}\left(\frac{1}{S}\right)$. The term $R\frac{\partial}{\partial p}\left(\frac{1}{S}\right)$ can be understood as the radiative-cooling driven convergence. Only above the maximum of $\frac{1}{S}$ (i.e., when $\frac{\partial}{\partial p}\left(\frac{1}{S}\right) > 0$), the cooling can contribute to the convergence. Notably, the climate impacts of $\frac{1}{S}\frac{\partial R}{\partial p}$ on the anvil height and amount have been well understood (Zelinka and Hartmann, 2010; Bony et al., 2016), whereas constant $R\frac{\partial}{\partial p}\left(\frac{1}{S}\right)$ is and its climate impacts have been barely known. In this case, the changes in the clear-sky convergence might not be fully predicted by the variation of the gradient of radiative cooling or the variation of S. Instead, C_{max} in the upper troposphere should be contributed by the collective impacts from the peak of radiative cooling and its maximum gradient. And the convergence driven by either the radiative cooling or its gradient is constrained by the stability profiles. Consequently, the primary clear-sky convergence might be constrained between the levels of the maximum of $\frac{1}{S}$ and $\frac{\partial}{\partial p}\left(\frac{1}{S}\right)$. This is consistent with the stability constraint on the anvil production in the cloudy sky (Figure 1a-d and Figure 2a-c). This consistency for the heights of convergence and divergence conforms to the mass conservation.

https://doi.org/10.5194/egusphere-2026-3420
Preprint. Discussion started: 6 July 2026

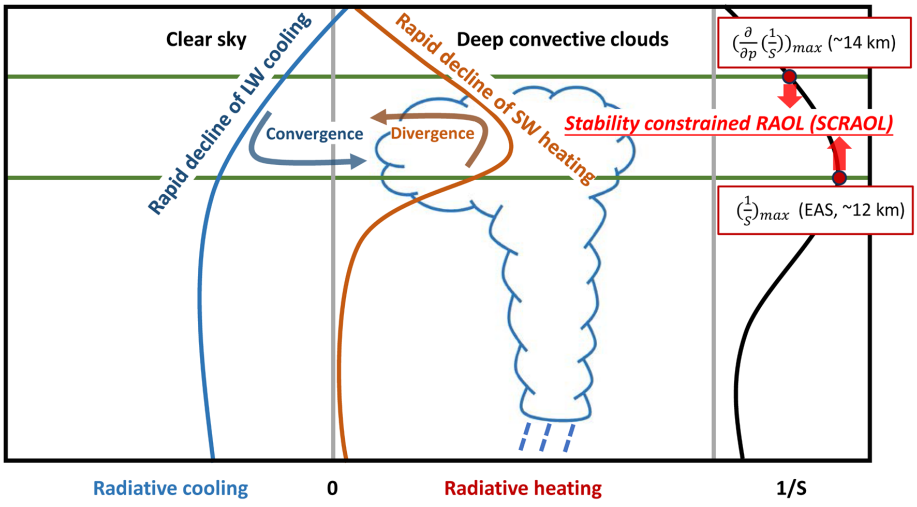

Figure 3. Illustration of the refined SCRAOL hypothesis for the non-precipitating anvil outflow. The primary radiation-driven anvil outflow and clear-sky convergence are both constrained between the levels of the maximum of $\frac{1}{S}$ and $\frac{\partial}{\partial p}\left(\frac{1}{S}\right)$.

Overall, as conceptualized in Figure 3 at the equilibrium state, the anvil outflow can be directly explained by the coupling of the convection, radiation and environmental stability, or indirectly diagnosed from the clear-sky convergence by the mass conservation. Grounded on the anvil outflow process hypothesized in Lilly (1988), the stability constraint on the RAOL is further clarified as shown in Figure 3. Owing to the transition from the convection-controlled to the radiation-controlled regimes vertically, the stability has a minimum in the upper troposphere (i.e., the maximum of $\frac{1}{S}$) and its gradient has a peak for the maximum of $\frac{\partial}{\partial p}\left(\frac{1}{S}\right)$. The anvil outflow driven by the radiative destabilization and heating are constrained by $\frac{1}{S}$ and $\frac{\partial}{\partial p}\left(\frac{1}{S}\right)$, respectively. Thus, when the convection overshoots between the levels of the maximum of $\frac{1}{S}$ and $\frac{\partial}{\partial p}\left(\frac{1}{S}\right)$, the radiation-driven anvil outflow at the convection top can be the strongest. Accordingly, the SCRAOL is formed between the levels of the maximum of $\frac{1}{S}$ and $\frac{\partial}{\partial p}\left(\frac{1}{S}\right)$ as shown in Figure 3. Away from this layer, anvil production is suppressed by the environmental stability. Similarly, the primary clear-sky convergence is also constrained between the levels of the maximum of $\frac{1}{S}$ and $\frac{\partial}{\partial p}\left(\frac{1}{S}\right)$. Notably, for either the cloudy or clear sky, the heights of the maximum of $\frac{1}{S}$ and $\frac{\partial}{\partial p}\left(\frac{1}{S}\right)$ barely change but with strong variations for their strength (shown Figure 1a and 1e), which is consistent with that in Wang and Yuan (2025). This implies that the stability constrains the cloudy-sky divergence and the clear-sky convergence at similar heights to explain the mass conservation.

4. Smaller or upward-shifting minimum stability can lift the tropical anvil clouds

As discussed above, the SCRAOL suggests that the primary radiation-driven anvil outflow is constrained between the levels of the maximum of $\frac{1}{S}$ and $\frac{\partial}{\partial p}\left(\frac{1}{S}\right)$. When the convection overshoots the level of the minimum stability, the anvil production is the most efficient and the anvil amount and structure is largely determined by the coupling impacts of the radiation and environmental stability. To validate this process, based on the GATM dataset, Figure 4 further shows how the SCRAOL constrains the anvil outflow when convection develops at different heights from 7 km to 18 km.

https://doi.org/10.5194/egusphere-2026-3420
Preprint. Discussion started: 6 July 2026

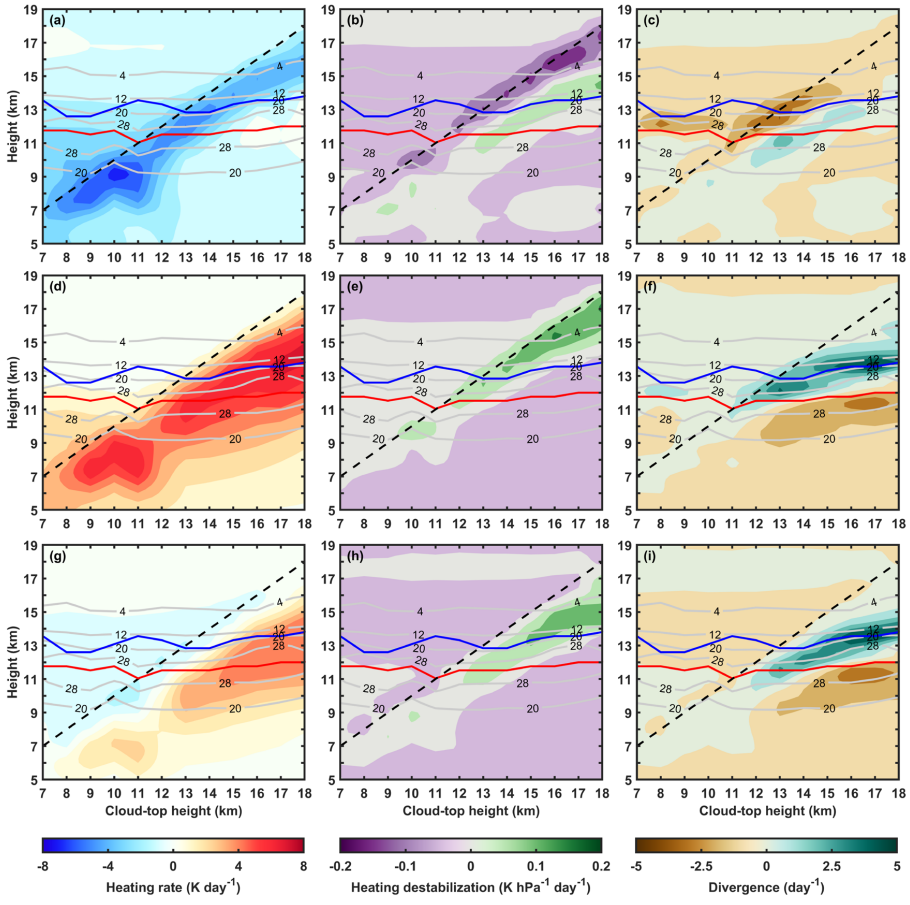

Figure 4. Vertical structures of stability, radiative heating and divergence for clouds at different heights. (a)-(c) radiative heating rates, radiative heating destabilization and divergence caused by LW radiation, respectively. (d)-(f) and (g)-(i) are similar to (a)-(c), but for SW and net radiation, respectively. The solid black contours represent $\frac{1}{S}$, with the units of K^{-1} hPa. The dash lines represent the location of the cloud-top height.

For the radiative heating structure, the LW (Figure 4a-b), SW (Figure 4d-e) and net (Figure 4g-h) radiative heating and destabilization are presented, respectively. In Figure 4a, 4d and 4g, convective clouds that develop at lower levels are accompanied with both strong LW cooling and SW heating, which leads to weak net heating. With convection developing to reach higher levels, LW cooling is reduced rapidly due to the decrease of temperature with height, whereas SW heating is less dependent on the atmospheric temperature and decreases relatively slowly. Ultimately, these high-topped clouds are more heated by net radiation stronger than low-topped clouds. Additionally, owing to the cancellation of strong cloud-top LW cooling with SW heating, the primary heating effect concentrates on the layer below the cloud top approximately 1-2 km. In Figure 4b, 4e and 4h, with convection developing from low to high levels, the strongest heating destabilizations of LW, SW and net radiation are all located at the level of approximately 1 km below the cloud top. It implies that, when convection develops to reach higher altitude, the location of the radiative heating and destabilization also increases to higher altitude, but is approximately constant relative to the cloud-top height. It implies that, the layer below the convective cloud top approximately 1-2 km is the most favorable for the outflow, if only considering the radiative impacts.

For the environmental thermal stratification ($\frac{1}{S}$, the black contours in Figure 4), the levels of the maximum of $\frac{1}{S}$ and

https://doi.org/10.5194/egusphere-2026-3420
Preprint. Discussion started: 6 July 2026

$\frac{\partial}{\partial p}\left(\frac{1}{S}\right)$ (the red and blue lines in Figure 4) are located at approximately 12 and 14 km, respectively, and do not vary with convection developing to reach a higher level. But higher-topped clouds seem to correspond to a greater peak value of $\frac{1}{S}$. It might be explained by the interaction between the environment and clouds. Less stable environment is favorable for the vertical development of clouds and radiative heating to clouds can further destabilize the environment.

Overall, the radiative heating and destabilization are closely associated with the convection development, whereas the levels of the maximum of $\frac{1}{S}$ and $\frac{\partial}{\partial p}\left(\frac{1}{S}\right)$ do not vary with convection development. The divergent outflow caused by the coupling of stability and LW, SW and net radiation are presented in Figure 4c, 4f and 4i, respectively. The outflow contributed by the coupling of stability and SW radiation is much stronger than that contributed by the LW radiation. When convection develop below the level of minimum stability (~12 km), the outflow is limited by strong environmental stability. When convective clouds develop to reach the SCRAOL between the maximum of $\frac{1}{S}$ and $\frac{\partial}{\partial p}\left(\frac{1}{S}\right)$ (~12-14 km), the anvil outflow is rapidly enhanced with the increase of SW radiative heating and destabilization and the decrease of stability, and the height of outflow also increases with clouds developing at higher altitude. Interestingly, when convective clouds develop from 14 km to 18 km, the height of the outflow does not increase with the rise of cloud top height and seems to be constant at approximately 14 km, although the SW radiative heating and destabilization is stronger at higher altitude (Figure 4f). When convective clouds develop above 14 km, the environmental thermal stratification is very stable to limit the radiation-driven anvil outflow. As a result, for these high-topped convective cloud bodies, their outflows are constrained by the environmental stability below 14 km. Ultimately, the main outflow level of the convective cloud body to form the anvil is primarily constrained by the SCRAOL between approximately 12 km and 14 km.

Consistently with previous studies (Chae and Sherwood, 2010; Zelinka and Hartmann, 2010), the level of the anvil outflow should be not completely fixed as hypothesized in the FAT but relies on the variation of stability. In Figure 5, the dependence of the anvil outflow on the stability is examined to validate this process. Here, as illustrated in Figure 5a, the main outflow level of clouds is regarded as the anvil and inferred by the level of the maximum cloud fraction (Z_{anvil}) based on the A-Train Constellation. Additionally, the minimum stability in the upper troposphere can be understood as the key stability of controlling the anvil outflow, which has been defined as the EAS in Wang and Yuan (2025). Wang and Yuan (2025) have shown that the EAS is strongly correlated with the high-level ice cloud amount. Here, the constraint of EAS and Z_{EAS} on the height of anvil outflow is primarily focused on. In Figure 5b, according to the PDF of EAS and Z_{EAS}, Z_{EAS} and EAS are independent and Z_{EAS} normally occurs between 10-14 km. Less stable environment (smaller EAS values) and higher Z_{EAS} contribute to higher Z_{anvil} and vice versa. This is well consistent with the SCRAOL:

(1) Less stable environment corresponds to larger $(\frac{1}{S})_{max}$ to allow stronger anvil outflow at higher levels;

(2) When the location of the minimum stability shifts upward, the environment at higher altitude is more supportive for the higher-level anvil outflow.

https://doi.org/10.5194/egusphere-2026-3420
Preprint. Discussion started: 6 July 2026

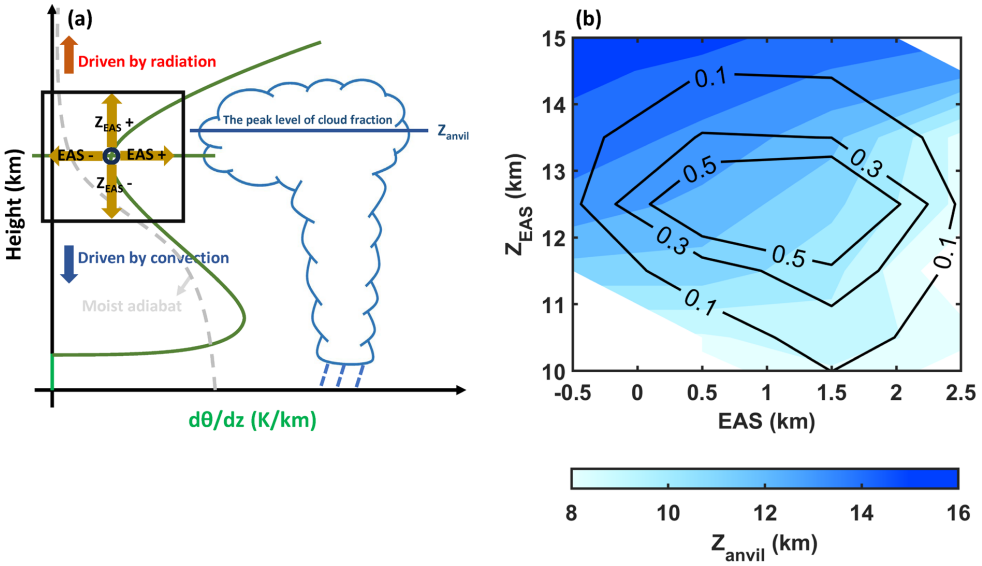

Figure 5. The implication of the SCRAOL for the stability controlling the level of anvil outflow. (a) Illustration of the physical meanings of the EAS, Z_{EAS} and the anvil outflow (Z_{anvil}). (b) Mean Z_{anvil} detected by CALIOP and CPR over the CERES footprint, under different thermodynamical conditions of EAS and Z_{EAS}. The black contours are the PDF of EAS and Z_{EAS}, which is normalized by dividing the maximum number.

5 Conclusion

By combining the GEO of identifying convection producing anvil clouds and the A-Train polar-orbit satellites of detecting the cross section of the radiation heating the anvil, the anvil outflow and its radiative interaction can be resolved from observations to refine the previously recognized process of anvil outflow dynamics. Consistently with the previously recognized anvil outflow process (Lilly, 1988; Wang, 2025), the LW cooling and SW heating both can destabilize the cloud top to promote the anvil outflow. On the other hand, the further refined anvil outflow process recognized through satellite observations manifests:

(1) The SW radiation heating anvil clouds seems to be more important than the cloud-top radiative destabilization for driving the daytime anvil outflow;

(2) The impact of either the LW or SW radiation on the anvil outflow is strongly constrained by the environmental stability and its gradient, which explains why the convection needs to overshoot the level of the minimum stability to be driven by radiation for the anvil spread.

According to the refined anvil outflow process, the SCRAOL is defined between the minimum stability and the maximum stability gradient, approximately 12-14 km. It represents the stability constraint on the anvil-radiation interaction. In the SCRAOL, the radiation can strongly interact with the anvil to drive the outflow. But away from this layer vertically, the anvil outflow and its interaction with radiation would be limited. Further observations demonstrate that less stable or upward-shifting SCRAOL can make the anvil production at a higher level.

The SCRAOL provides a refined key physical process for the feedback among convection, radiation and environment. It links the convective anvil structure driven by radiation to the changes in the environmental thermal stratification. A more (less) stable environment can suppress (promote) the anvil production at a lower (higher) level, which can further modulate the radiative energy budget. This anvil outflow process refined from satellite observations may provide new understandings

https://doi.org/10.5194/egusphere-2026-3420
Preprint. Discussion started: 6 July 2026

on how anvil clouds are produced from convection and how it responds to the climatic environmental change.

Acknowledgments

The author declares no conflict of interest. This work was supported by the State Key Laboratory of Severe Weather Meteorological Science and Technology (2025KFB09) and The Scientific Research Startup Foundation for Introduced Talents of Nanjing University of Information Science and Technology.

Competing interests.

The contact author has declared that none of the authors has any competing interests.

Author contributions.

ZW prepared the original manuscript.

Data and code availability

All data used in this study are available online. The GEO images are obtained from the National Aeronautics and Space Administration (NASA) Langley Research Center Atmospheric Science Data Center (https://doi.org/10.5067/MTS01/CERES, NASA/LARC/SD/ASDC, 2017). The GPM is obtained from the Goddard Earth Sciences Data and Information Services Center (GES DISC) at https://doi.org/10.5067/GPM/IMERG/3BHH/07 (Huffman et al., 2023). The CCCM data product are obtained from the National Aeronautics and Space Administration (NASA) Langley Research Center Atmospheric Science Data Center (https://search.earthdata.nasa.gov/). The ERA5 reanalysis used in this study is available through Hersbach et al. (2020) from the ECMWF (DOI: https://doi.org/10.24381/cds.bd0915c6) and available at https://cds.climate.copernicus.eu/datasets/reanalysis-era5-pressure-levels?tab=overview.

The code is available upon request.

References

Atlas, R. L., Bretherton, C. S., Sokol, A. B., Blossey, P. N., and Khairoutdinov, M. F.: Tropical Cirrus Are Highly Sensitive to Ice Microphysics Within a Nudged Global Storm-Resolving Model, Geophysical Research Letters, 51, e2023GL105868, 10.1029/2023gl105868, 2024.

Babu, S. R.: Convective tropopause over the tropics: Climatology, seasonality, and inter-annual variability inferred from long-term FORMOSAT-3/COSMIC-1 RO data, Atmospheric Research, 298, 107159, https://doi.org/10.1016/j.atmosres.2023.107159, 2024.

Berry, E. and Mace, G. G.: Cloud properties and radiative effects of the Asian summer monsoon derived from A-Train data, Journal of Geophysical Research: Atmospheres, 119, 9492-9508, 10.1002/2014jd021458, 2014.

Biondi, R., Randel, W. J., Ho, S. P., Neubert, T., and Syndergaard, S.: Thermal structure of intense convective clouds derived from GPS radio occultations, Atmos. Chem. Phys., 12, 5309-5318, 10.5194/acp-12-5309-2012, 2012.

Blossey, P. N., Bretherton, C. S., Cetrone, J., and Kharoutdinov, M.: Cloud-Resolving Model Simulations of KWAJEX: Model Sensitivities and Comparisons with Satellite and Radar Observations, Journal of the Atmospheric Sciences, 64, 1488-1508, 10.1175/jas3982.1, 2007.

Bony, S., Stevens, B., Coppin, D., Becker, T., Reed, K. A., Voigt, A., and Medeiros, B.: Thermodynamic control of anvil cloud amount, Proc Natl Acad Sci U S A, 113, 8927-8932, 10.1073/pnas.1601472113, 2016.

Bretherton, C. S.: Insights into low-latitude cloud feedbacks from high-resolution models, Philos Trans A Math Phys Eng Sci, 373, 20140415, 10.1098/rsta.2014.0415, 2015.

Chae, J. H. and Sherwood, S. C.: Insights into Cloud-Top Height and Dynamics from the Seasonal Cycle of Cloud-Top Heights

https://doi.org/10.5194/egusphere-2026-3420
Preprint. Discussion started: 6 July 2026

Observed by MISR in the West Pacific Region, Journal of the Atmospheric Sciences, 67, 248-261, 10.1175/2009jas3099.1, 2010.

Clement, A. C. and Soden, B.: The Sensitivity of the Tropical-Mean Radiation Budget, Journal of Climate, 18, 3189-3203, 10.1175/jcli3456.1, 2005.

Del Genio, A. D. and Kovari, W.: Climatic Properties of Tropical Precipitating Convection under Varying Environmental Conditions, Journal of Climate, 15, 2597-2615, https://doi.org/10.1175/1520-0442(2002)015<2597:CPOTPC>2.0.CO;2, 2002.

Deng, M., Mace, G. G., and Wang, Z.: Anvil Productivities of Tropical Deep Convective Clusters and Their Regional Differences, Journal of the Atmospheric Sciences, 73, 3467-3487, https://doi.org/10.1175/JAS-D-15-0239.1, 2016.

Feng, Z., Leung, L. R., Houze, R. A., Hagos, S., Hardin, J., Yang, Q., Han, B., and Fan, J.: Structure and Evolution of Mesoscale Convective Systems: Sensitivity to Cloud Microphysics in Convection-Permitting Simulations Over the United States, Journal of Advances in Modeling Earth Systems, 10, 1470-1494, 10.1029/2018ms001305, 2018.

Folkins, I.: Origin of Lapse Rate Changes in the Upper Tropical Troposphere, Journal of the Atmospheric Sciences, 59, 992-1005, 10.1175/1520-0469(2002)059<0992:Oolrci>2.0.Co;2, 2002.

Folkins, I. and Martin, R. V.: The Vertical Structure of Tropical Convection and Its Impact on the Budgets of Water Vapor and Ozone, Journal of the Atmospheric Sciences, 62, 1560-1573, 10.1175/jas3407.1, 2005.

Gasparini, B., Blossey, P. N., Hartmann, D. L., Lin, G., and Fan, J.: What Drives the Life Cycle of Tropical Anvil Clouds?, Journal of Advances in Modeling Earth Systems, 11, 2586-2605, 10.1029/2019ms001736, 2019.

Gasparini, B., Rasch, P. J., Hartmann, D. L., Wall, C. J., and Dütsch, M.: A Lagrangian Perspective on Tropical Anvil Cloud Lifecycle in Present and Future Climate, Journal of Geophysical Research: Atmospheres, 126, e2020JD033487, 10.1029/2020jd033487, 2021.

Gettelman, A. and Forster, P. M. d. F.: A Climatology of the Tropical Tropopause Layer, Journal of the Meteorological Society of Japan. Ser. II, 80, 911-924, 10.2151/jmsj.80.911, 2002.

Gray, W. M. and Jacobson, R. W.: Diurnal Variation of Deep Cumulus Convection, Monthly Weather Review, 105, 1171-1188, 10.1175/1520-0493(1977)105<1171:Dvodcc>2.0.Co;2, 1977.

Hartmann, D. L.: Tropical anvil clouds and climate sensitivity, Proceedings of the National Academy of Sciences, 113, 8897-8899, 10.1073/pnas.1610455113, 2016.

Hartmann, D. L. and Berry, S. E.: The balanced radiative effect of tropical anvil clouds, J Geophys Res-Atmos, 122, 5003-5020, 10.1002/2017jd026460, 2017.

Hartmann, D. L. and Larson, K.: An important constraint on tropical cloud - climate feedback, Geophysical Research Letters, 29, 1951, 10.1029/2002gl015835, 2002.

Hersbach, H., Bell, B., Berrisford, P., Hirahara, S., Horányi, A., Muñoz-Sabater, J., Nicolas, J., Peubey, C., Radu, R., Schepers, D., Simmons, A., Soci, C., Abdalla, S., Abellan, X., Balsamo, G., Bechtold, P., Biavati, G., Bidlot, J., Bonavita, M., Chiara, G., Dahlgren, P., Dee, D., Diamantakis, M., Dragani, R., Flemming, J., Forbes, R., Fuentes, M., Geer, A., Haimberger, L., Healy, S., Hogan, R. J., Hólm, E., Janisková, M., Keeley, S., Laloyaux, P., Lopez, P., Lupu, C., Radnoti, G., Rosnay, P., Rozum, I., Vamborg, F., Villaume, S., and Thépaut, J. N.: The ERA5 global reanalysis, Quarterly Journal of the Royal Meteorological Society, 146, 1999-2049, 10.1002/qj.3803, 2020.

Houze, R. A.: Mesoscale convective systems, Reviews of Geophysics, 42, RG4003, 10.1029/2004rg000150, 2004.

Igel, M. R., Drager, A. J., and van den Heever, S. C.: A CloudSat cloud object partitioning technique and assessment and integration of deep convective anvil sensitivities to sea surface temperature, Journal of Geophysical Research: Atmospheres, 119, 10515-10535, 10.1002/2014jd021717, 2014.

Kato, S., Sun-Mack, S., Miller, W. F., Rose, F. G., Chen, Y., Minnis, P., and Wielicki, B. A.: Relationships among cloud occurrence frequency, overlap, and effective thickness derived from CALIPSO and CloudSat merged cloud vertical profiles, Journal of Geophysical Research: Atmospheres, 115, D00H28, 10.1029/2009jd012277, 2010.

Kato, S., Rose, F. G., Sun-Mack, S., Miller, W. F., Chen, Y., Rutan, D. A., Stephens, G. L., Loeb, N. G., Minnis, P., Wielicki, B. A., Winker, D. M., Charlock, T. P., Stackhouse Jr., P. W., Xu, K.-M., and Collins, W. D.: Improvements of top-of-atmosphere

https://doi.org/10.5194/egusphere-2026-3420
Preprint. Discussion started: 6 July 2026

and surface irradiance computations with CALIPSO-, CloudSat-, and MODIS-derived cloud and aerosol properties, Journal of Geophysical Research: Atmospheres, 116, D19209, https://doi.org/10.1029/2011JD016050, 2011.

Kiehl, J. T.: On the Observed Near Cancellation between Longwave and Shortwave Cloud Forcing in Tropical Regions, Journal of Climate, 7, 559-565, 10.1175/1520-0442(1994)007<0559:Otoncb>2.0.Co;2, 1994.

L'Ecuyer, T. S. and Jiang, J. H.: Touring the atmosphere aboard the A-Train, Physics Today, 63, 36-41, 10.1063/1.3463626, 2010.

Lilly, D. K.: Cirrus Outflow Dynamics, Journal of the Atmospheric Sciences, 45, 1594-1605, 10.1175/1520-0469(1988)045<1594:Cod>2.0.Co;2, 1988.

Lindzen, R. S., Chou, M.-D., and Hou, A. Y.: Does the Earth Have an Adaptive Infrared Iris?, Bulletin of the American Meteorological Society, 82, 417-432, 10.1175/1520-0477(2001)082<0417:Dtehaa>2.3.Co;2, 2001.

Mapes, B. E. and Houze, R. A.: Diabatic Divergence Profiles in Western Pacific Mesoscale Convective Systems, Journal of the Atmospheric Sciences, 52, 1807-1828, 10.1175/1520-0469(1995)052<1807:Ddpiwp>2.0.Co;2, 1995.

Matsui, T., Zeng, X., Tao, W.-K., Masunaga, H., Olson, W. S., and Lang, S.: Evaluation of Long-Term Cloud-Resolving Model Simulations Using Satellite Radiance Observations and Multifrequency Satellite Simulators, Journal of Atmospheric and Oceanic Technology, 26, 1261-1274, 10.1175/2008jtecha1168.1, 2009.

Mauritsen, T. and Stevens, B.: Missing iris effect as a possible cause of muted hydrological change and high climate sensitivity in models, Nature Geoscience, 8, 346-351, 10.1038/ngeo2414, 2015.

Moorthi, S. and Suarez, M. J.: Relaxed Arakawa-Schubert. A Parameterization of Moist Convection for General Circulation Models, Monthly Weather Review, 120, 978-1002, https://doi.org/10.1175/1520-0493(1992)120<0978:RASAPO>2.0.CO;2, 1992.

Nicholls, M. E.: An investigation of how radiation may cause accelerated rates of tropical cyclogenesis and diurnal cycles of convective activity, Atmos. Chem. Phys., 15, 9003-9029, 10.5194/acp-15-9003-2015, 2015.

Powell, S. W., Houze, R. A., Kumar, A., and McFarlane, S. A.: Comparison of Simulated and Observed Continental Tropical Anvil Clouds and Their Radiative Heating Profiles, Journal of the Atmospheric Sciences, 69, 2662-2681, 10.1175/jas-d-11-0251.1, 2012.

Raghuraman, S. P., Medeiros, B., and Gettelman, A.: Observational Quantification of Tropical High Cloud Changes and Feedbacks, Journal of Geophysical Research: Atmospheres, 129, e2023JD039364, https://doi.org/10.1029/2023JD039364, 2024.

Rennó, N. O., Emanuel, K. A., and Stone, P. H.: Radiative-convective model with an explicit hydrologic cycle: 1. Formulation and sensitivity to model parameters, Journal of Geophysical Research: Atmospheres, 99, 14429-14441, 10.1029/94jd00020, 1994.

Riihimaki, L. D. and McFarlane, S. A.: Frequency and morphology of tropical tropopause layer cirrus from CALIPSO observations: Are isolated cirrus different from those connected to deep convection?, Journal of Geophysical Research: Atmospheres, 115, https://doi.org/10.1029/2009JD013133, 2010.

Saint-Lu, M., Bony, S., and Dufresne, J.-L.: Observational Evidence for a Stability Iris Effect in the Tropics, Geophysical Research Letters, 47, e2020GL089059, https://doi.org/10.1029/2020GL089059, 2020.

Saint-Lu, M., Bony, S., and Dufresne, J. L.: Observational Evidence for a Stability Iris Effect in the Tropics, Geophysical Research Letters, 47, 10.1029/2020gl089059, 2020.

Schooley, A. H.: Wake Collapse in a Stratified Fluid, Science, 157, 421-423, doi:10.1126/science.157.3787.421, 1967.

Seeley, J. T., Jeevanjee, N., Langhans, W., and Romps, D. M.: Formation of Tropical Anvil Clouds by Slow Evaporation, Geophysical Research Letters, 46, 492-501, https://doi.org/10.1029/2018GL080747, 2019.

Sobel, A. H., Nilsson, J., and Polvani, L. M.: The Weak Temperature Gradient Approximation and Balanced Tropical Moisture Waves, Journal of the Atmospheric Sciences, 58, 3650-3665, https://doi.org/10.1175/1520-0469(2001)058<3650:TWTGAA>2.0.CO;2, 2001.

Sokol, A. B., Wall, C. J., and Hartmann, D. L.: Greater climate sensitivity implied by anvil cloud thinning, Nature Geoscience,

https://doi.org/10.5194/egusphere-2026-3420
Preprint. Discussion started: 6 July 2026

17, 398-403, 10.1038/s41561-024-01420-6, 2024.

Stephens, G. L., Vane, D. G., Boain, R. J., Mace, G. G., Sassen, K., Wang, Z., Illingworth, A. J., O'Connor, E. J., Rossow, W. B., Durden, S. L., Miller, S. D., Austin, R. T., Benedetti, A., and Mitrescu, C.: The Cloudsat Mission and the a-Train, Bulletin of the American Meteorological Society, 83, 1771-1790, 10.1175/bams-83-12-1771, 2002.

Sunilkumar, S. V., Babu, A., and Parameswaran, K.: Mean structure of the tropical tropopause and its variability over the Indian longitude sector, Climate Dynamics, 40, 1125-1140, 10.1007/s00382-012-1496-8, 2013.

Sunilkumar, S. V., Muhsin, M., Venkat Ratnam, M., Parameswaran, K., Krishna Murthy, B. V., and Emmanuel, M.: Boundaries of tropical tropopause layer (TTL): A new perspective based on thermal and stability profiles, Journal of Geophysical Research: Atmospheres, 122, 741-754, 10.1002/2016jd025217, 2017.

Suzuki, K., Golaz, J. C., and Stephens, G. L.: Evaluating cloud tuning in a climate model with satellite observations, Geophysical Research Letters, 40, 4464-4468, 10.1002/grl.50874, 2013.

Thompson, D. W. J., Bony, S., and Li, Y.: Thermodynamic constraint on the depth of the global tropospheric circulation, Proc Natl Acad Sci U S A, 114, 8181-8186, 10.1073/pnas.1620493114, 2017.

Wall, C. J., Hartmann, D. L., Thieman, M. M., Smith, W. L., and Minnis, P.: The Life Cycle of Anvil Clouds and the Top-of-Atmosphere Radiation Balance over the Tropical West Pacific, Journal of Climate, 31, 10059-10080, 10.1175/jcli-d-18-0154.1, 2018.

Wall, C. J., Norris, J. R., Gasparini, B., Smith, W. L., Thieman, M. M., and Sourdeval, O.: Observational Evidence that Radiative Heating Modifies the Life Cycle of Tropical Anvil Clouds, Journal of Climate, 33, 8621-8640, 10.1175/jcli-d-20-0204.1, 2020.

Wang, Z.: Anvil–radiation diurnal interaction: shortwave radiative-heating destabilization driving the diurnal variation of convective anvil outflow and its modulation on the radiative cancellation, Atmos. Chem. Phys., 25, 5021-5039, 10.5194/acp-25-5021-2025, 2025.

Wang, Z. and Yuan, J.: Observing convective activities in complex convective organizations and their contributions to precipitation and anvil cloud amounts, Atmos. Chem. Phys., 24, 13811-13831, 10.5194/acp-24-13811-2024, 2024.

Wang, Z. and Yuan, J.: A Novel Thermodynamical Predictor of Tropical High-Cloud Area Coverage: Estimated Anvil-Outflow Stability, Geophysical Research Letters, 52, e2025GL115026, https://doi.org/10.1029/2025GL115026, 2025.

Xian, T. and Fu, Y.: Characteristics of tropopause-penetrating convection determined by TRMM and COSMIC GPS radio occultation measurements, Journal of Geophysical Research: Atmospheres, 120, 7006-7024, https://doi.org/10.1002/2014JD022633, 2015.

Xu, K. M., Cederwall, R. T., Donner, L. J., Grabowski, W. W., Guichard, F., Johnson, D. E., Khairoutdinov, M., Krueger, S. K., Petch, J. C., Randall, D. A., Seman, C. J., Tao, W. K., Wang, D., Cheng Xie, S., Yio, J. J., and Zhang, M. H.: An intercomparison of cloud-resolving models with the atmospheric radiation measurement summer 1997 intensive observation period data, Quarterly Journal of the Royal Meteorological Society, 128, 593-624, 10.1256/003590002321042117, 2006.

Yin, J. and Porporato, A.: Radiative effects of daily cycle of cloud frequency in past and future climates, Climate Dynamics, 54, 1625-1637, 10.1007/s00382-019-05077-5, 2019.

Yuan, J. and Houze, R. A.: Global Variability of Mesoscale Convective System Anvil Structure from A-Train Satellite Data, Journal of Climate, 23, 5864-5888, 10.1175/2010jcli3671.1, 2010.

Yuan, J., Houze, R. A., and Heymsfield, A. J.: Vertical Structures of Anvil Clouds of Tropical Mesoscale Convective Systems Observed by CloudSat, Journal of the Atmospheric Sciences, 68, 1653-1674, 10.1175/2011jas3687.1, 2011.

Zelinka, M. D. and Hartmann, D. L.: Why is longwave cloud feedback positive?, Journal of Geophysical Research, 115, D16117, 10.1029/2010jd013817, 2010.

Zhao, M.: An Investigation of the Connections among Convection, Clouds, and Climate Sensitivity in a Global Climate Model, Journal of Climate, 27, 1845-1862, 10.1175/jcli-d-13-00145.1, 2014.

Zhao, M., Golaz, J. C., Held, I. M., Ramaswamy, V., Lin, S. J., Ming, Y., Ginoux, P., Wyman, B., Donner, L. J., Paynter, D., and Guo, H.: Uncertainty in Model Climate Sensitivity Traced to Representations of Cumulus Precipitation Microphysics,

https://doi.org/10.5194/egusphere-2026-3420
Preprint. Discussion started: 6 July 2026

Journal of Climate, 29, 543-560, 10.1175/jcli-d-15-0191.1, 2016.

Zheng, Y., Jeevanjee, N., Lin, P., Paynter, D., and Tan, Z.: Physics or Knob-Tuning? Tropical Anvil Peak Is Captured by GCMs, Geophysical Research Letters, 52, e2025GL118740, https://doi.org/10.1029/2025GL118740, 2025.

Notably, for the cloudy sky, the diabatic heating (Q) in Eq. 2 is the sum of radiative heating and latent heating, whose contributions to D seem to be independent. For the cloudy sky, the radiative heating coupled with stability can be understood as the environmental control on divergence, whereas the latent heating coupled with stability represents the control of cloud microphysical processes on divergence. In this work, only the roles of environmental stability and radiation in spreading tropical high clouds are investigated.